

**Boundary Perturbation Methods for High–Frequency Acoustic Scattering:
Shallow Periodic Gratings**

David P. Nicholls^{a)}

*Department of Mathematics,
Statistics,
and Computer Science,
University of Illinois at Chicago,
Chicago,
IL 60607*

Fernando Reitich^{b)}

*School of Mathematics,
University of Minnesota,
Minneapolis,
MN 55455*

(Dated: February 1, 2008)

Abstract

Despite significant recent advances in numerical methodologies for simulating rough-surface acoustic scattering, their applicability has been constrained by the limitations of state-of-the-art computational resources. This has been particularly true in high-frequency applications where the sheer size of the full-wave simulations render them impractical, and engineering processes must therefore rely on asymptotic models (e.g., Kirchhoff approximation-KA-). However, the demands for high precision can make the latter inappropriate, thus efficient, error-controllable methodologies must be devised. This paper presents a computational strategy that combines the virtues of rigorous solvers (error control) with those of high-frequency asymptotic models (frequency-independent computational costs). These methods are based on *high-order* “boundary perturbations” which display high precision and unparalleled efficiency. This is accomplished by incorporating asymptotic phase information to effect a significant decrease in computational effort while retaining the full-wave nature of the approach. The developments of this contribution are constrained to configurations that preclude multiple scattering; it is further explained how the schemes can be made applicable to general scattering scenarios, though implementation details are left for future work. Even for single-scattering configurations, the approach presented here gives significant gains in accuracy when compared to asymptotic theories (e.g., KA) with modest additional computational cost.

PACS numbers: 43.20.-f, 43.20.Bi, 43.20.El, 43.20.Fn, 43.30.Hw

I. INTRODUCTION

The significant advances in high-performance algorithms and hardware that have been attained over the last three decades have had a substantial impact on the classical engineering and design paradigm of repeated physical experimentation, interpretation, and modification in the most varied applications. Those relating to wave dynamics (e.g., acoustic, electromagnetic, elastic), such as in remote sensing¹, nondestructive testing², or imaging³, for instance, have increasingly relied on *numerical* simulations to accelerate assessment and/or prototyping projects. The success of such strategies has, in turn, provided further impetus to continue to migrate towards virtual experimentation and it has thus enhanced the need for evermore efficient and accurate simulators. These needs are, however, challenged by the increasing complexity of the processes to be numerically represented which continuously test the limits of state-of-the-art computational methodologies and platforms. In the context of wave propagation these complexities can arise from that of the geometrical arrangement, from the intrinsic oscillations of the field quantities, or from both. Current simulation capabilities allow for the treatment of complicated geometries with a high degree of detail and accuracy. It is thus the requirement to resolve field quantities on the scale of the wavelength of oscillation that typically limits the applicability of advanced simulation schemes, and that consistently results in the need to abandon these in favor of approximate (high-frequency) asymptotic theories.

In this paper we introduce a family of numerical algorithms that are designed to overcome these limitations while avoiding the inaccuracies that arise (at finite frequencies) from asymptotic solutions, such as those based on the classical Kirchhoff approximation⁴ (KA) or on its corrected versions⁵⁻⁸. The schemes we present are based on *high-order* “boundary perturbations” (see, e.g., [9-16] and the references therein) and can therefore be made to approximate the exact solution of full-wave scattering models to within any prescribed ac-

^{a)}Electronic address: nicholls@math.uic.edu

^{b)}Electronic address: reitich@math.umn.edu

curacy. As in classical implementations of these methods, the procedures we introduce here display a high degree of precision (owing to their spectral nature), and efficiency (stemming from the use of accelerated evaluations, e.g., based on FFTs). In contrast with the classical approach, however, these characteristics are attained here while avoiding the need to discretize the fields on the scale of the wavelength.

The basic observation that allows for such discretizations, and the consequent reduction in computational cost, relates to the possibility of predetermining the manner in which field quantities oscillate. More precisely, asymptotic high-frequency theories (e.g. geometrical acoustics) can be used *a priori* to predict the *phase* of the fields and, thus, to reduce the number of unknowns through its extraction, leaving only a slowly oscillatory modulation to be found. In the simplest case of impenetrable scatterers and wherein waves do not undergo multiple reflections, for instance, this phase takes on a particularly uncomplicated form, given by that of the incoming radiation on the surface of the obstacles and by the classical law of reflection away from these. This idea of “phase extraction” has been extensively used in the design of low-order analytical scattering theories (see, e.g., [5, 8, 17–20]) and, more recently, in the solution of integral equation formulations^{21–25}. Here, in contrast, we explain how this can be incorporated into classical boundary perturbation algorithms to allow for efficient solutions of arbitrary accuracy.

Unlike low-order theories, the schemes we present here produce solutions that actually converge to that of the full-wave model. In fact, this characteristic also contrasts our approach with the high-order solutions of [21–23] which can be shown to be only asymptotic. Our methodology is perhaps most closely related to the work in [24, 25] which introduces a *rigorous* approach to the numerical solution of high-frequency scattering problems based on the idea of phase extraction. This latter work is concerned with bounded scatterers for which an integral equation solver is designed to produce solutions with any prescribed accuracy in frequency-independent computational times. To this end, and in addition to the extraction of the phase, the work introduces suitable numerical mechanisms for a high-order treatment of the resulting singular and high-frequency integration problems as well as of

shadowing transitions²⁴ and multiple scattering effects²⁵. While a similar approach, based on integral equations, is certainly viable for the case we consider here of infinite (periodic) rough surfaces, the alternative perturbative procedures we advocate display some distinct advantages. In particular, for instance, these latter methodologies obviate the need to deal with the complications brought about by the corresponding Green’s function (related to cost of its evaluation²⁶), which are exacerbated at high frequencies, or with those related to the evaluation of oscillatory integrals²⁵.

Although the derivations that follow apply to every boundary perturbation approach, for the sake of definiteness we shall detail these for two particularly popular schemes, namely the “Field Expansions” (FE) method of Bruno & Reitich^{9–11} (a high–order, analytically continued version of the classical Rayleigh–Rice theory^{27,28}); and the “Operator Expansion” (OE) method of Milder^{29–33} (based on perturbative expansions of the Dirichlet–Neumann Operator–DNO–). In this initial contribution we constrain our developments to configurations that preclude multiple scattering, and are thus readily comparable with classical high–frequency approximations (e.g., KA). Extensions to cases wherein the effects of multiple scattering are significant can be attained through an iterative procedure that successfully accounts for secondary reflections²⁵. The numerical implementation of this procedure, however, is significantly more complicated (as it does, for instance, require the development of an accurate geometrical acoustics solver) and it is thus left for future work.

With these considerations, the rest of the paper is organized as follows: First, and for the sake of completeness, in § II we recall the governing equations of rough surface scattering. Then, in § III, we introduce the high–frequency versions of the OE and FE approaches that incorporate (single scattering) phase information to greatly reduce the number of degrees of freedom that are necessary to approximate the solution to any given accuracy. In § IV we display results of numerical simulations which substantiate these claims and which show, in particular, that the approach can deliver significantly improved results when compared to classical asymptotic theories (e.g., KA) at a very modest additional computational cost. Finally, our conclusions follow in § V.

II. GOVERNING EQUATIONS

The problem we consider is the scattering of time-harmonic acoustic waves from an impenetrable infinite surface which, for simplicity, is “sound soft” (our methods are easily modified to deal with other boundary conditions). We will consider the general three-dimensional case with crossed periodic gratings having shape represented by $y = g(x_1, x_2)$ where $g(x_1 + d_1, x_2 + d_2) = g(x_1, x_2)$ for periods d_1 and d_2 .

If an incident plane-wave

$$v_i(x_1, x_2, y) = e^{i(\alpha x_1 + \beta x_2 - \gamma y)},$$

is incident on the surface, then this problem is governed by the Helmholtz equation with quasi-periodic lateral boundary conditions and a pressure release boundary condition at the scatterer, i.e.,

$$\Delta v + k^2 v = 0 \quad y > g(x_1, x_2) \quad (1a)$$

$$v(x_1, x_2, g(x_1, x_2)) = -v_i(x_1, x_2, g(x_1, x_2)) =: \xi(x_1, x_2) \quad (1b)$$

$$v(x_1 + d_1, x_2 + d_2, y) = e^{i(\alpha d_1 + \beta d_2)} v(x_1, x_2, y), \quad (1c)$$

where v is the scattered field, ξ will denote the boundary data, and $k^2 = \alpha^2 + \beta^2 + \gamma^2$. To specify a unique solution of (1) we need a boundary condition at infinity; this is given by an upward propagating condition³⁴ which states that all scattered waves are “outgoing.” It can be shown^{15,16} that this can be explicitly enforced in the near-field with a “transparent boundary condition” at a hyperplane $y = a > \max |g|$. More precisely, (1) is equivalent to:

$$\Delta v + k^2 v = 0 \quad g(x_1, x_2) < y < a \quad (2a)$$

$$v(x_1, x_2, g(x_1, x_2)) = \xi(x_1, x_2) \quad (2b)$$

$$\partial_y v(x_1, x_2, a) - T[v(x_1, x_2, a)] = 0 \quad (2c)$$

$$v(x_1 + d_1, x_2 + d_2, y) = e^{i(\alpha d_1 + \beta d_2)} v(x_1, x_2, y), \quad (2d)$$

where

$$T[\psi] := \sum_{p_1=-\infty}^{\infty} \sum_{p_2=-\infty}^{\infty} (i\gamma_{p_1, p_2}) \hat{\psi}_{p_1, p_2} e^{i(\alpha_{p_1} x_1 + \beta_{p_2} x_2)},$$

and

$$\alpha_{p_1} = \alpha + (2\pi/d_1)p_1, \quad \beta_{p_2} = \beta + (2\pi/d_2)p_2, \quad \gamma_{p_1, p_2} = \sqrt{k^2 - \alpha_{p_1}^2 - \beta_{p_2}^2}, \quad (3)$$

and $\text{Im}\{\gamma_{p_1, p_2}\} \geq 0$. In this formula we have used the (generalized) Fourier series representation for quasi-periodic functions:

$$\psi(x_1, x_2) = \sum_{p_1=-\infty}^{\infty} \sum_{p_2=-\infty}^{\infty} \hat{\psi}_{p_1, p_2} e^{i(\alpha_{p_1} x_1 + \beta_{p_2} x_2)}. \quad (4)$$

Once computed, we can use the scattered field v to realize any of several near- and far-field quantities of interest. In the present context we will consider the normal derivative of the field at the surface of the scatterer:

$$\nu(x_1, x_2) := [\nabla v \cdot N_g]_{y=g}$$

where $N_g = (\partial_{x_1} g, \partial_{x_2} g, -1)^T$ is an exterior normal to the physical domain of the problem. As the “input” to our problem is the Dirichlet data ξ and the “output” is the Neumann information ν , this map is oftentimes called the Dirichlet–Neumann operator^{15,16} (DNO), or Dirichlet–to–Neumann map^{35,36}. We will denote this DNO by:

$$G(g)[\xi] := [\nabla v \cdot N_g]_{y=g} = [-\partial_y v + (\partial_{x_1} g) \partial_{x_1} v + (\partial_{x_2} g) \partial_{x_2} v]_{y=g}. \quad (5)$$

We note that knowledge of the DNO is exactly equivalent to that of the full solution to the scattering problem (2), as the field at any point can be readily recovered from this and the boundary pressure via Green’s identities.

III. BOUNDARY PERTURBATION METHODS

The power and simplicity of Boundary Perturbation (BP) methods are based upon viewing the complicated problem domain as a perturbation of a much simpler one where the solution is trivial to compute. In the present context we view the shape of the grating, g , as a perturbation of a flat configuration, $g = \varepsilon f$ where, at the outset, ε will be small. Based upon this identification, one makes expansions of the form, e.g.,

$$v(x_1, x_2, y, \varepsilon) = \sum_{n=0}^{\infty} v_n(x_1, x_2, y) \varepsilon^n, \quad G(\varepsilon f)[\xi] = \sum_{n=0}^{\infty} G_n(f)[\xi] \varepsilon^n, \quad (6)$$

which can subsequently be shown to be *strongly convergent* under quite general conditions^{16,37}. Additionally, these solutions can typically be continued analytically^{16,38} so that, in fact, ε can be chosen quite large (provided that it remains real). In a numerical implementation this fact can be used to advantage if a suitable analytic continuation technique, such as Padé approximation³⁹, is utilized. As we shall see, this combination of ideas leads to algorithms with quite remarkable properties of reliability, cost-effectiveness, and high-order accuracy.

A. Field Expansions

The derivation of the Field Expansions (FE) method (originally named the “Method of Variation of Boundaries”^{9–11}) begins with the expansion of the field, v :

$$v = v(x_1, x_2, y, \varepsilon) = \sum_{n=0}^{\infty} v_n(x_1, x_2, y) \varepsilon^n.$$

Upon insertion into (2) and evaluation at matching powers of ε , we realize the following system of equations to be solved:

$$\Delta v_n + k^2 v_n = 0 \quad 0 < y < a \quad (7a)$$

$$v_n(x_1, x_2, 0) = P_n(x_1, x_2) \quad (7b)$$

$$\partial_y v_n(x_1, x_2, a) - T[v_n(x_1, x_2, a)] = 0 \quad (7c)$$

$$v_n(x_1 + d_1, x_2 + d_2, y) = e^{i(\alpha d_1 + \beta d_2)} v_n(x_1, x_2, y), \quad (7d)$$

where

$$P_n(x_1, x_2) = \delta_{n,0} \xi(x_1, x_2) - \sum_{l=0}^{n-1} F_{n-l}(x_1, x_2) \partial_y^{n-l} v_l(x_1, x_2, 0),$$

and

$$F_l(x_1, x_2) := \frac{f(x_1, x_2)^l}{l!}.$$

We recall that solutions v_n of (7a), (7c), & (7d) can be written as

$$v_n(x_1, x_2, y) = \sum_{p_1=-\infty}^{\infty} \sum_{p_2=-\infty}^{\infty} d_{p_1, p_2, n} e^{i(\alpha p_1 x_1 + \beta p_2 x_2 + \gamma p_1 \cdot p_2 y)}, \quad (8)$$

c.f. (3). Given that ξ can be expressed as:

$$\xi(x_1, x_2) = \sum_{p_1=-\infty}^{\infty} \sum_{p_2=-\infty}^{\infty} \hat{\xi}_{p_1, p_2} e^{i(\alpha_{p_1} x_1 + \beta_{p_2} x_2)},$$

c.f. (4), (7b) delivers a recursion formula for the $d_{p_1, p_2, n}$:

$$d_{p_1, p_2, n} = \delta_{n,0} \hat{\xi}_{p_1, p_2} - \sum_{l=0}^{n-1} \sum_{q_1=-\infty}^{\infty} \sum_{q_2=-\infty}^{\infty} F_{n-l, p_1-q_1, p_2-q_2} (i\gamma_{q_1, q_2})^{n-l} d_{q_1, q_2, l}, \quad (9)$$

where the coefficients F_{l, p_1, p_2} are defined by

$$F_l(x_1, x_2) =: \sum_{p_1=-\infty}^{\infty} \sum_{p_2=-\infty}^{\infty} F_{l, p_1, p_2} e^{i((2\pi/d_1)p_1 x_1 + (2\pi/d_2)p_2 x_2)}.$$

To compute the DNO, (5), we note that

$$\begin{aligned} \sum_{n=0}^{\infty} G_n(f)[\xi] \varepsilon^n &= G(\varepsilon f)[\xi] = [-\partial_y v + (\varepsilon \partial_{x_1} f) \partial_{x_1} v + (\varepsilon \partial_{x_2} f) \partial_{x_2} v]_{y=\varepsilon f} \\ &= \sum_{n=0}^{\infty} \varepsilon^n \sum_{p_1=-\infty}^{\infty} \sum_{p_2=-\infty}^{\infty} (-i\gamma_{p_1, p_2} + (\varepsilon \partial_{x_1} f) i\alpha_{p_1} + (\varepsilon \partial_{x_2} f) i\beta_{p_2}) \\ &\quad \times d_{p_1, p_2, n} e^{i(\alpha_{p_1} x_1 + \beta_{p_2} x_2 + \gamma_{p_1, p_2} \varepsilon f)}. \end{aligned}$$

From this we deduce that

$$\begin{aligned} G_n(f) &= \sum_{p_1=-\infty}^{\infty} \sum_{p_2=-\infty}^{\infty} \left(-\sum_{l=0}^n F_{n-l} (i\gamma_{p_1, p_2})^{n-l+1} d_{p_1, p_2, l} \right. \\ &\quad \left. + \sum_{l=0}^{n-1} F_{n-l-1} ((\partial_{x_1} f)(i\alpha_{p_1}) + (\partial_{x_2} f)(i\beta_{p_2})) (i\gamma_{p_1, p_2})^{n-l-1} d_{p_1, p_2, l} \right) e^{i(\alpha_{p_1} x_1 + \beta_{p_2} x_2)}. \quad (10) \end{aligned}$$

B. High Frequency Field Expansions

As we shall see in § IV.A, the FE method we have just described is not particularly well-suited for high-frequency simulations. If the Fourier-Taylor coefficients $d_{p_1, p_2, n}$ from (9) are truncated after $N_{x_1} \times N_{x_2}$ Fourier modes and N Taylor terms, then the FE method has quite modest time ($\mathcal{O}(N_{x_1} \log(N_{x_1}) N_{x_2} \log(N_{x_2}) N)$) and memory ($\mathcal{O}(N_{x_1} N_{x_2} N)$) requirements. However, *all* features of the the scattered field must be resolved to realize an accurate solution and, for this, the number of Fourier terms $N_{x_1} \times N_{x_2}$ *must* scale like $k \times k$.

However, the technique of “phase extraction”^{5,8,19,21,22} gives us insight into how one can create an FE method which *is* specially designed for high–frequency calculations. In the present context, and in the absence of multiple scattering, it can be shown (see, e.g., [24, 40]) that:

$$\nu(x_1, x_2) = e^{i(\alpha x_1 + \beta x_2 - \gamma g(x_1, x_2))} \mu(x_1, x_2), \quad (11)$$

where μ is a “slowly varying” envelope whose variations *do not* accentuate with increasing frequency. Note that this implies, in particular, that a uniformly accurate representation of μ can be attained with a number of degrees of freedom that is independent of the wavenumber k . Motivated by this realization we factor the *field*

$$v(x_1, x_2, y) = e^{i(\alpha x_1 + \beta x_2 - \gamma y)} w(x, y)$$

and substitute this into (2) which delivers

$$\Delta w + 2i(\alpha, \beta, -\gamma) \cdot \nabla w = 0 \quad g(x) < y < a \quad (12a)$$

$$w(x_1, x_2, g(x_1, x_2)) = -1 \quad (12b)$$

$$w(x_1 + d_1, x_2 + d_2, y) = w(x_1, x_2, y). \quad (12c)$$

For the condition at the artificial boundary $y = a$, c.f. (2c), we begin with the calculation:

$$\begin{aligned} v(x_1, x_2, a) &= e^{i(\alpha x_1 + \beta x_2)} e^{-ia\gamma} w(x_1, x_2, a) \\ &= e^{-ia\gamma} e^{i(\alpha x_1 + \beta x_2)} \sum_{p_1=-\infty}^{\infty} \sum_{p_2=-\infty}^{\infty} \tilde{d}_{p_1, p_2} e^{i((2\pi/d_1)p_1 x_1 + (2\pi/d_2)p_2 x_2)} \\ &= e^{-ia\gamma} \sum_{p_1=-\infty}^{\infty} \sum_{p_2=-\infty}^{\infty} \tilde{d}_{p_1, p_2} e^{i(\alpha p_1 x_1 + \beta p_2 x_2)}, \end{aligned}$$

where

$$\tilde{d}_{p_1, p_2} := \frac{1}{d_1 d_2} \int_0^{d_1} \int_0^{d_2} w(x_1, x_2, a) e^{-i((2\pi/d_1)p_1 x_1 + (2\pi/d_2)p_2 x_2)} dx_1 dx_2$$

is the (p_1, p_2) -th Fourier coefficient of $w(x_1, x_2, a)$. Now, applying the operator T :

$$\begin{aligned}
T[v(x_1, x_2, a)] &= e^{-ia\gamma} T \left[\sum_{p_1=-\infty}^{\infty} \sum_{p_2=-\infty}^{\infty} \tilde{d}_{p_1, p_2} e^{i(\alpha p_1 x_1 + \beta p_2 x_2)} \right] \\
&= e^{-ia\gamma} \sum_{p_1=-\infty}^{\infty} \sum_{p_2=-\infty}^{\infty} (i\gamma_{p_1, p_2}) \tilde{d}_{p_1, p_2} e^{i(\alpha p_1 x_1 + \beta p_2 x_2)} \\
&= e^{i(\alpha x_1 + \beta x_2)} e^{-ia\gamma} \sum_{p_1=-\infty}^{\infty} \sum_{p_2=-\infty}^{\infty} (i\gamma_{p_1, p_2}) \tilde{d}_{p_1, p_2} e^{i((2\pi/d_1)p_1 x_1 + (2\pi/d_2)p_2 x_2)}.
\end{aligned}$$

Finally, (2c) gives

$$\begin{aligned}
0 &= \partial_y v(x_1, x_2, a) - T[v(x_1, x_2, a)] \\
&= \left(\partial_y w(x_1, x_2, a) - \sum_{p_1=-\infty}^{\infty} \sum_{p_2=-\infty}^{\infty} (i\gamma_{p_1, p_2} + i\gamma) \tilde{d}_{p_1, p_2} e^{i((2\pi/d_1)p_1 x_1 + (2\pi/d_2)p_2 x_2)} \right) \\
&\quad \times e^{i(\alpha x_1 + \beta x_2)} e^{-ia\gamma},
\end{aligned}$$

and we realize

$$\partial_y w(x_1, x_2, a) - T_0[w(x_1, x_2, a)] = 0, \quad (13)$$

where, for a *periodic* function $\zeta(x_1, x_2)$,

$$T_0[\zeta(x_1, x_2)] := \sum_{p_1=-\infty}^{\infty} \sum_{p_2=-\infty}^{\infty} (i\gamma_{p_1, p_2} + i\gamma) \hat{\zeta}_{p_1, p_2} e^{i((2\pi/d_1)p_1 x_1 + (2\pi/d_2)p_2 x_2)}. \quad (14)$$

Again, it can be shown that the (factored) field w can be expanded in a convergent Taylor series

$$w = w(x_1, x_2, y, \varepsilon) = \sum_{n=0}^{\infty} w_n(x_1, x_2, y) \varepsilon^n.$$

These w_n must satisfy

$$\Delta w_n + 2i(\alpha, \beta, -\gamma) \cdot \nabla w_n = 0 \quad 0 < y < a \quad (15a)$$

$$w_n(x_1, x_2, 0) = Q_n(x_1, x_2) \quad (15b)$$

$$\partial_y w_n(x_1, x_2, a) - T_0[w_n(x_1, x_2, a)] = 0 \quad (15c)$$

$$w_n(x_1 + d_1, x_2 + d_2, y) = w_n(x_1, x_2, y), \quad (15d)$$

where

$$Q_n(x_1, x_2) = -\delta_{n,0} - \sum_{l=0}^{n-1} F_{n-l}(x_1, x_2) \partial_y^{n-l} w_l(x_1, x_2, 0).$$

Solutions of (15a), (15c), & (15d) are given by

$$w_n(x_1, x_2, y) = \sum_{p_1=-\infty}^{\infty} \sum_{p_2=-\infty}^{\infty} b_{p_1, p_2, n} e^{(i\gamma p_1, p_2 + i\gamma)y} e^{i((2\pi/d_1)p_1 x_1 + (2\pi/d_2)p_2 x_2)},$$

so that (15b) gives

$$b_{p_1, p_2, n} = -\delta_{n,0} \delta_{p_1,0} \delta_{p_2,0} - \sum_{l=0}^{n-1} \sum_{q_1=-\infty}^{\infty} \sum_{q_2=-\infty}^{\infty} F_{n-l, p_1-q_1, p_2-q_2} (i\gamma_{q_1, q_2} + i\gamma)^{n-l} b_{q_1, q_2, l}, \quad (16)$$

c.f. (9).

To compute the DNO we recall our factorization, (11), of the “fast” surface velocity ν as the product of an oscillatory term and a “slow” surface velocity μ . In terms of the “slow” field, w , we can write

$$\begin{aligned} \mu(x_1, x_2) &= e^{i(-\alpha x_1 - \beta x_2 + \gamma g(x_1, x_2))} \nu(x_1, x_2) \\ &= e^{i(-\alpha x_1 - \beta x_2 + \gamma g(x_1, x_2))} [-\partial_y v + (\partial_{x_1} g) \partial_{x_1} v + (\partial_{x_2} g) \partial_{x_2} v]_{y=g} \\ &= e^{i(-\alpha x_1 - \beta x_2 + \gamma g(x_1, x_2))} [(i\gamma) e^{i(\alpha x_1 + \beta x_2 - \gamma y)} w - e^{i(\alpha x_1 + \beta x_2 - \gamma y)} \partial_y w \\ &\quad + (\partial_{x_1} g) (i\alpha) e^{i(\alpha x_1 + \beta x_2 - \gamma y)} w + (\partial_{x_2} g) (i\beta) e^{i(\alpha x_1 + \beta x_2 - \gamma y)} w \\ &\quad + (\partial_{x_1} g) e^{i(\alpha x_1 + \beta x_2 - \gamma y)} \partial_{x_1} w + (\partial_{x_2} g) e^{i(\alpha x_1 + \beta x_2 - \gamma y)} \partial_{x_2} w]_{y=g} \\ &= [(i\gamma) w - \partial_y w + (\partial_{x_1} g) (i\alpha) w + (\partial_{x_2} g) (i\beta) w + (\partial_{x_1} g) \partial_{x_1} w + (\partial_{x_2} g) \partial_{x_2} w]_{y=g}. \end{aligned}$$

Now, if the w depends analytically upon ε then so will

$$\tilde{G}(\varepsilon f)[\psi(x_1, x_2)] := e^{i(-\alpha x_1 - \beta x_2 + \gamma \varepsilon f(x_1, x_2))} G(\varepsilon f) [e^{i(\alpha x_1 + \beta x_2 - \gamma \varepsilon f(x_1, x_2))} \psi(x_1, x_2)], \quad (17)$$

where $\psi \equiv -1$ corresponds to plane-wave scattering, i.e. $\tilde{G}(\varepsilon f)[-1] = \mu(x)$. Thus

$$\begin{aligned} \sum_{n=0}^{\infty} \tilde{G}_n(f) \varepsilon^n &= \tilde{G}(\varepsilon f)[-1] = [(i\gamma) w - \partial_y w + ((\varepsilon \partial_{x_1} f) (i\alpha) + (\varepsilon \partial_{x_2} f) (i\beta)) w \\ &\quad + (\varepsilon \partial_{x_1} f) \partial_{x_1} w + (\varepsilon \partial_{x_2} f) \partial_{x_2} w]_{y=g} \\ &= \sum_{n=0}^{\infty} \varepsilon^n \sum_{p_1=-\infty}^{\infty} \sum_{p_2=-\infty}^{\infty} [i\gamma - (i\gamma_{p_1, p_2} + i\gamma) + (\varepsilon \partial_{x_1} f) i\alpha + (\varepsilon \partial_{x_2} f) i\beta \\ &\quad + (\varepsilon \partial_{x_1} f) i(2\pi/d_1) p_1 + (\varepsilon \partial_{x_2} f) i(2\pi/d_2) p_2] \\ &\quad \times b_{p_1, p_2, n} e^{i((2\pi/d_1)p_1 x_1 + (2\pi/d_2)p_2 x_2 + (\gamma + \gamma_{p_1, p_2}) \varepsilon f)}. \end{aligned}$$

From this we have

$$\begin{aligned}
\tilde{G}_n(f) = & \sum_{p_1=-\infty}^{\infty} \sum_{p_2=-\infty}^{\infty} \left(\sum_{l=0}^n F_{n-l}(i\gamma)(i\gamma_{p_1,p_2} + i\gamma)^{n-l} b_{p_1,p_2,l} \right. \\
& - \sum_{l=0}^n F_{n-l}(i\gamma_{p_1,p_2} + i\gamma)^{n-l+1} b_{p_1,p_2,l} \\
& + \sum_{l=0}^{n-1} F_{n-l-1} [(\partial_{x_1} f)(i\alpha) + (\partial_{x_2} f)(i\beta)] (i\gamma_{p_1,p_2} + i\gamma)^{n-l-1} b_{p_1,p_2,l} \\
& \left. + \sum_{l=0}^{n-1} F_{n-l-1} [(\partial_{x_1} f)i((2\pi/d_1)p_1) + (\partial_{x_2} f)i(2\pi/d_2)p_2] (i\gamma_{p_1,p_2} + i\gamma)^{n-l-1} b_{p_1,p_2,l} \right). \quad (18)
\end{aligned}$$

To reconstruct the DNO we simply multiply each of the \tilde{G}_n by the factor $\exp(i(\alpha x_1 + \beta x_2 - \gamma g(x_1, x_2)))$.

C. Operator Expansions

Milder's "Operator Expansions" (OE) method²⁹⁻³³, is a somewhat different approach than the FE algorithm as it endeavors to compute, given Dirichlet data, *only* the normal derivative (the DNO). Of course, as we mentioned, if the full field is desired then an appropriate integral can be used to recover this. To specify this OE algorithm we begin with the observation that the function

$$u_p(x, y) = e^{i(\alpha_{p_1} x_1 + \beta_{p_2} x_2 + \gamma_{p_1,p_2} y)}$$

satisfies (2a), (2c), & (2d). Recalling the definition of the DNO, (5), and, again, setting $g(x_1, x_2) = \varepsilon f(x_1, x_2)$, we observe that

$$\begin{aligned}
G(\varepsilon f) [e^{i(\alpha_{p_1} x_1 + \beta_{p_2} x_2 + \gamma_{p_1,p_2} \varepsilon f(x_1, x_2))}] \\
= (-i\gamma_{p_1,p_2} + \varepsilon(\partial_{x_1} f)(i\alpha_{p_1}) + \varepsilon(\partial_{x_2} f)(i\beta_{p_2})) e^{i(\alpha_{p_1} x_1 + \beta_{p_2} x_2 + \gamma_{p_1,p_2} \varepsilon f(x_1, x_2))}. \quad (19)
\end{aligned}$$

Our goal is to, once again, take advantage of the analyticity properties of the DNO to find the Neumann data. This requires a formula for the n -th term in the expansion of the DNO, G_n , c.f. (6), as applied to a generic quasi-periodic function $\xi(x_1, x_2)$. Making use of the

representation

$$\xi(x_1, x_2) = \sum_{p_1=-\infty}^{\infty} \sum_{p_2=-\infty}^{\infty} \hat{\xi}_{p_1, p_2} e^{i(\alpha_{p_1} x_1 + \beta_{p_2} x_2)}, \quad (20)$$

c.f. (4), it suffices to find a formula for G_n applied to a single harmonic $\exp(i(\alpha_{p_1} x_1 + \beta_{p_2} x_2))$.

For this we use (19):

$$\begin{aligned} & \left(\sum_{n=0}^{\infty} \varepsilon^n G_n(f) \right) \left[e^{i(\alpha_{p_1} x_1 + \beta_{p_2} x_2)} \sum_{n=0}^{\infty} F_n(i\gamma_{p_1, p_2})^n \varepsilon^n \right] \\ &= (-i\gamma_{p_1, p_2} + \varepsilon(\partial_{x_1} f)(i\alpha_{p_1}) + \varepsilon(\partial_{x_2} f)(i\beta_{p_2})) e^{i(\alpha_{p_1} x_1 + \beta_{p_2} x_2)} \sum_{n=0}^{\infty} F_n(i\gamma_{p_1, p_2})^n \varepsilon^n, \end{aligned}$$

where, again, $F_l := f^l/l!$. At order ε^0 we find:

$$G_0 [e^{i(\alpha_{p_1} x_1 + \beta_{p_2} x_2)}] = -i\gamma_{p_1, p_2} e^{i(\alpha_{p_1} x_1 + \beta_{p_2} x_2)},$$

which, using (20), gives

$$G_0 [\xi] = -i\gamma_D \xi := \sum_{p_1=-\infty}^{\infty} \sum_{p_2=-\infty}^{\infty} (-i\gamma_{p_1, p_2}) \hat{\xi}_{p_1, p_2} e^{i(\alpha_{p_1} x_1 + \beta_{p_2} x_2)},$$

and defines the order-one Fourier multiplier G_0 . At order ε^n , $n \geq 1$, we have:

$$\begin{aligned} G_n(f) [e^{i(\alpha_{p_1} x_1 + \beta_{p_2} x_2)}] &= -F_n(i\gamma_{p_1, p_2})^{n+1} e^{i(\alpha_{p_1} x_1 + \beta_{p_2} x_2)} \\ &+ [(\partial_{x_1} f)F_{n-1}(i\alpha_{p_1}) + (\partial_{x_2} f)F_{n-1}(i\beta_{p_2})] (i\gamma_{p_1, p_2})^{n-1} e^{i(\alpha_{p_1} x_1 + \beta_{p_2} x_2)} \\ &- \sum_{l=0}^{n-1} G_l(f) [F_{n-l}(i\gamma_{p_1, p_2})^{n-l} e^{i(\alpha_{p_1} x_1 + \beta_{p_2} x_2)}]. \end{aligned}$$

We can simplify the first two terms

$$\begin{aligned} R_n &:= -F_n(i\gamma_{p_1, p_2})^{n+1} e^{i(\alpha_{p_1} x_1 + \beta_{p_2} x_2)} + (\partial_{x_1} f)F_{n-1}(i\alpha_{p_1})(i\gamma_{p_1, p_2})^{n-1} e^{i(\alpha_{p_1} x_1 + \beta_{p_2} x_2)} \\ &+ (\partial_{x_2} f)F_{n-1}(i\beta_{p_2})(i\gamma_{p_1, p_2})^{n-1} e^{i(\alpha_{p_1} x_1 + \beta_{p_2} x_2)} \\ &= \{-F_n(i\gamma_{p_1, p_2})^2 + (\partial_{x_1} f)F_{n-1}(i\alpha_{p_1}) + (\partial_{x_2} f)F_{n-1}(i\beta_{p_2})\} (i\gamma_{p_1, p_2})^{n-1} e^{i(\alpha_{p_1} x_1 + \beta_{p_2} x_2)} \end{aligned}$$

with the observation that, since $\alpha_{p_1}^2 + \beta_{p_2}^2 + \gamma_{p_1, p_2}^2 = k^2$, we have

$$\begin{aligned} R_n &= \{F_n k^2 + F_n(i\alpha_{p_1})^2 + F_n(i\beta_{p_2})^2 + (\partial_{x_1} f)F_{n-1}(i\alpha_{p_1}) + (\partial_{x_2} f)F_{n-1}(i\beta_{p_2})\} (i\gamma_{p_1, p_2})^{n-1} \\ &\times e^{i(\alpha_{p_1} x_1 + \beta_{p_2} x_2)}. \end{aligned}$$

Rewriting this using differential operators and the product rule we realize

$$\begin{aligned} R_n &= (F_n k^2 + F_n \partial_{x_1}^2 + F_n \partial_{x_2}^2 + (\partial_{x_1} f) F_{n-1} \partial_{x_1} + (\partial_{x_2} f) F_{n-1} \partial_{x_2}) (i\gamma_D)^{n-1} e^{i(\alpha_{p_1} x_1 + \beta_{p_2} x_2)} \\ &= (F_n k^2 + \partial_{x_1} F_n \partial_{x_1} + \partial_{x_2} F_n \partial_{x_2}) (i\gamma_D)^{n-1} e^{i(\alpha_{p_1} x_1 + \beta_{p_2} x_2)}, \end{aligned}$$

resulting in

$$\begin{aligned} G_n(f) [\xi] &= k^2 F_n (i\gamma_D)^{n-1} \xi + \partial_{x_1} F_n \partial_{x_1} (i\gamma_D)^{n-1} \xi + \partial_{x_2} F_n \partial_{x_2} (i\gamma_D)^{n-1} \xi \\ &\quad - \sum_{l=0}^{n-1} G_l(f) [F_{n-l} (i\gamma_D)^{n-l} \xi], \end{aligned} \tag{21}$$

where we have again used (20).

D. High Frequency Operator Expansions

In a manner similar to that outlined in § III.B we can design a high-frequency OE method by making use of the factorization (11). For this “High Frequency Operator Expansions” (HFOE) method we wish to work directly with the DNO, however, now it should be scaled by the incident radiation so that it is slowly varying. Again, our goal is to find a formula for the n -th term in the expansion acting on an *arbitrary* function. However, our surface function is the *periodic*, factored (slowly varying) incident radiation

$$\psi(x_1, x_2) := e^{i(-\alpha x_1 - \beta x_2 + \gamma g(x_1, x_2))} \xi(x_1, x_2) = -1.$$

Of course, this has a trivial Fourier series

$$\psi(x_1, x_2) = \hat{\psi}_{0,0} e^{i(0x_1 + 0x_2)} = (-1) e^{i(0x_1 + 0x_2)},$$

but we find it convenient to find the action of the n -th term in the expansion of the reduced DNO applied to a general Fourier mode $\exp(i((2\pi/d_1)p_1 x_1 + (2\pi/d_2)p_2 x_2))$.

As before, c.f. (17), we claim that $\tilde{G}(\varepsilon f)$ depends analytically upon ε , so that

$$\tilde{G}(\varepsilon f) = \sum_{n=0}^{\infty} \tilde{G}_n(f) \varepsilon^n.$$

To derive an explicit recurrence for the operators $\tilde{G}_n(f)$, we set

$$\psi(x_1, x_2) = e^{i((2\pi/d_1)p_1x_1 + (2\pi/d_2)p_2x_2 + \gamma g(x_1, x_2) + \gamma_{p_1, p_2}g(x_1, x_2))}. \quad (22)$$

Using this and the definition, (17), we find

$$\begin{aligned} \tilde{G}(g)[\psi] &= e^{i(-\alpha x_1 - \beta x_2 + \gamma g(x_1, x_2))} G(g) [e^{i(\alpha_{p_1} x_1 + \beta_{p_2} x_2 + \gamma_{p_1, p_2} g(x_1, x_2))}] \\ &= e^{i(-\alpha x_1 - \beta x_2 + \gamma g(x_1, x_2))} [-\partial_y v(x_1, x_2, y) + (\partial_{x_1} g) \partial_{x_1} v(x_1, x_2, y) \\ &\quad + (\partial_{x_2} g) \partial_{x_2} v(x_1, x_2, y)]_{y=g}, \end{aligned}$$

since the Dirichlet data, (22), we provide to G gives rise to the exact solution:

$$v(x_1, x_2, y) = e^{i(\alpha_{p_1} x_1 + \beta_{p_2} x_2 + \gamma_{p_1, p_2} y)}.$$

Continuing,

$$\begin{aligned} \tilde{G}(\varepsilon f)[\psi] &= e^{i(-\alpha x_1 - \beta x_2 + \gamma \varepsilon f(x_1, x_2))} (-i\gamma_{p_1, p_2} + (\varepsilon \partial_{x_1} f)(i\alpha_{p_1}) + (\varepsilon \partial_{x_2} f)(i\beta_{p_2})) \\ &\quad \times e^{i(\alpha_{p_1} x_1 + \beta_{p_2} x_2 + \gamma_{p_1, p_2} \varepsilon f(x_1, x_2))} \\ &= (-i\gamma_{p_1, p_2} + (\varepsilon \partial_{x_1} f)(i\alpha_{p_1}) + (\varepsilon \partial_{x_2} f)(i\beta_{p_2})) \\ &\quad \times e^{i(2\pi/d_1)p_1x_1 + i(2\pi/d_2)p_2x_2 + (i\gamma_{p_1, p_2} + i\gamma)\varepsilon f(x_1, x_2)}, \end{aligned}$$

c.f. (19). Expanding as we did in the previous section:

$$\begin{aligned} \left(\sum_{n=0}^{\infty} \varepsilon^n \tilde{G}_n(f) \right) &\left[e^{i((2\pi/d_1)p_1x_1 + (2\pi/d_2)p_2x_2)} \sum_{n=0}^{\infty} F_n(i\gamma_{p_1, p_2} + i\gamma)^n \varepsilon^n \right] \\ &= (-i\gamma_{p_1, p_2} + \varepsilon(\partial_{x_1} f)(i\alpha_{p_1}) + \varepsilon(\partial_{x_2} f)(i\beta_{p_2})) e^{i((2\pi/d_1)p_1x_1 + (2\pi/d_2)p_2x_2)} \\ &\quad \times \sum_{n=0}^{\infty} F_n(i\gamma_{p_1, p_2} + i\gamma)^n \varepsilon^n, \end{aligned}$$

we find that, at order zero,

$$\tilde{G}_0[\psi] = -(i\gamma_D)\psi,$$

and at order $n \geq 1$,

$$\begin{aligned} \tilde{G}_n[\psi] &= -F_n(i\gamma_D)(i\gamma_D + i\gamma)^n \psi + (\partial_{x_1} f) F_{n-1}(i\alpha_D)(i\gamma_D + i\gamma)^{n-1} \psi \\ &\quad + (\partial_{x_2} f) F_{n-1}(i\beta_D)(i\gamma_D + i\gamma)^{n-1} \psi - \sum_{l=0}^{n-1} \tilde{G}_l [F_{n-l}(i\gamma_D + i\gamma)^{n-l} \psi]. \quad (23) \end{aligned}$$

IV. NUMERICAL TESTS

In this section we illustrate the superior accuracy one can realize with our new algorithms with cost *independent* of the frequency. We begin with a series of numerical tests in two dimensions, § IV.A, where we consider gratings which are invariant in one direction and the incident field is aligned precisely so that this invariant direction can be ignored. This configuration can be simulated with the algorithms outlined above by simply setting $\beta = 0$, setting $d = d_1$, $x = x_1$, etc. In § IV.B we consider the full three-dimensional problem and show that our general conclusions are unchanged.

A. Two Dimensional Tests

To test the usefulness of the two new algorithms, HFFE and HFOE, outlined above we will use them to compute the induced normal surface velocity for two scatterers with very different smoothness. For simplicity we assume the period to be $d = 2\pi$, and we consider the following profiles^{15,16}: A sinusoid

$$f_s(x) = \cos(x), \tag{24a}$$

and a non-differentiable (“Lipschitz”) function

$$f_L(x) = \begin{cases} -(2/\pi)x + 1 & 0 \leq x \leq \pi \\ (2/\pi)x - 3 & \pi \leq x \leq 2\pi. \end{cases} \tag{24b}$$

For our simulations we point out that f_L admits an infinite Fourier series expansions¹⁵:

$$f_L(x) = \sum_{r=1}^{\infty} \frac{8}{\pi^2(2r-1)^2} \cos((2r-1)x),$$

which, in our numerical simulations, we will truncate after P terms:

$$f_{L,P}(x) = \sum_{r=1}^{P/2} \frac{8}{\pi^2(2r-1)^2} \cos((2r-1)x); \tag{25}$$

please see Figure 1 for depictions of (24a) and (25) ($P = 40$).

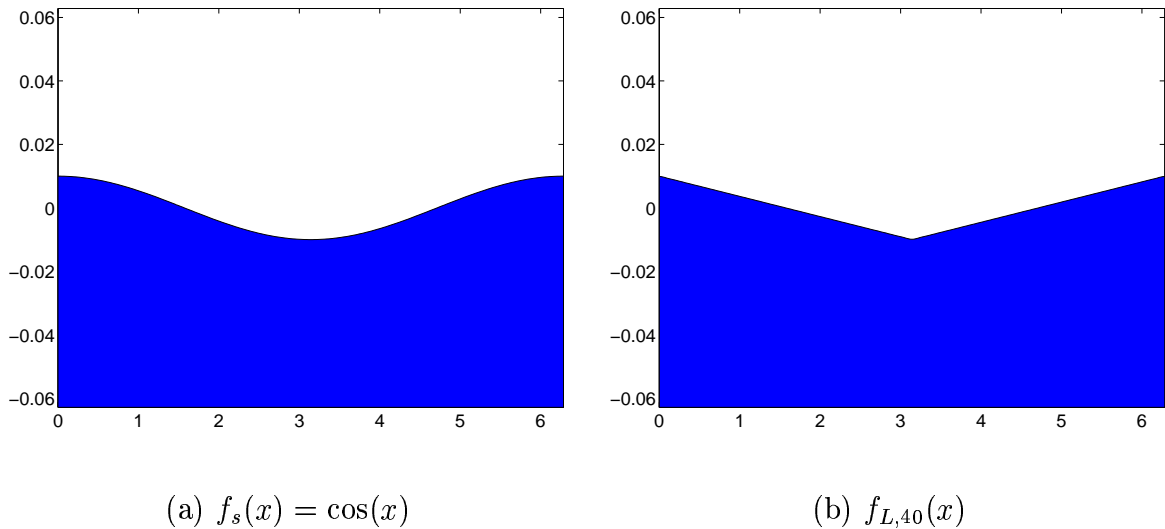


FIG. 1. Plots of the two-dimensional profiles $f_s(x) = \cos(x)$, (24a), and $f_{L,40}$, (25).

Of course, for a generic profile there is no exact closed-form solution to the problem of plane-wave scattering by a grating so we resort to an alternative method to produce an “exact solution” with which we can compare. For this purpose we use the reliable, high-order “Transformed Field Expansion” (TFE) method^{16,41} for very large and/or very rough scatterers. For all of the two-dimensional simulations we present, a highly resolved reference solution was produced using this TFE algorithm with $N_x = 1024$ (horizontal) Fourier modes, $N_y = 64$ (vertical) Chebyshev coefficients, and $N = 28$ Taylor orders; see [16] for a complete description of this method and these numerical parameters. These reference solutions can be shown to attain relative accuracies of the order of 10^{-10} which certainly suffice for our demonstration purposes. In this context then this becomes the smallest realizable “error,” though the actual solutions we compute can be significantly more accurate when compared to the actual exact solution.

In Tables I, II, & III we display results of FE, HFFE, OE, and HFOE simulations of plane-wave scattering from the sinusoidal profile, (24a), with $\varepsilon = 0.01$ (to exclude the possibility of multiple reflections) for $(\alpha, \gamma) = (1, 1)$, $(10, 10)$, and $(100, 100)$, respectively. To exemplify the capabilities of our new methods, in all of these simulations we fix the number of Fourier modes at $N_x = 16$ and study our solutions as the Taylor order is varied among

$N = 0, 2, 4, 6,$ and 8 . In this, and all future simulations, we have summed these Taylor series using Padé approximation³⁹ although, as the order N is quite small, the accuracy gains were typically modest.

In Table I we see that all four algorithms realize the optimal errors with respect to the TFE solution (of the order of 10^{-10}) by perturbation order $N = 6$ which is to be expected as this solution for $(\alpha, \gamma) = (1, 1)$ is not very oscillatory. However, for this discretization, the FE and OE algorithms produce inaccurate results for $(\alpha, \gamma) = (10, 10)$, and $(100, 100)$. Of course, this is not surprising as these algorithms attempt to resolve quite oscillatory functions with only $|r| < N_x/2 = 8$ modes. By contrast, as our new HFFE/HFOE methods simulate the *slowly* varying envelope μ , we notice *uniformly* excellent convergence behavior for all choices of (α, γ) where accuracies of 10^{-9} or 10^{-10} are always achieved with $N = 8$ perturbation orders. For this final frequency we also display a plot of the slow, $\mu(x)$, and fast, $\nu(x)$, surface velocities in Figure 2. From this we can clearly see how our new approach delivers such superior accuracy as the slowly changing function $\mu(x)$ can easily be represented with $N_x = 16$ which is obviously insufficient for the highly oscillatory $\nu(x)$.

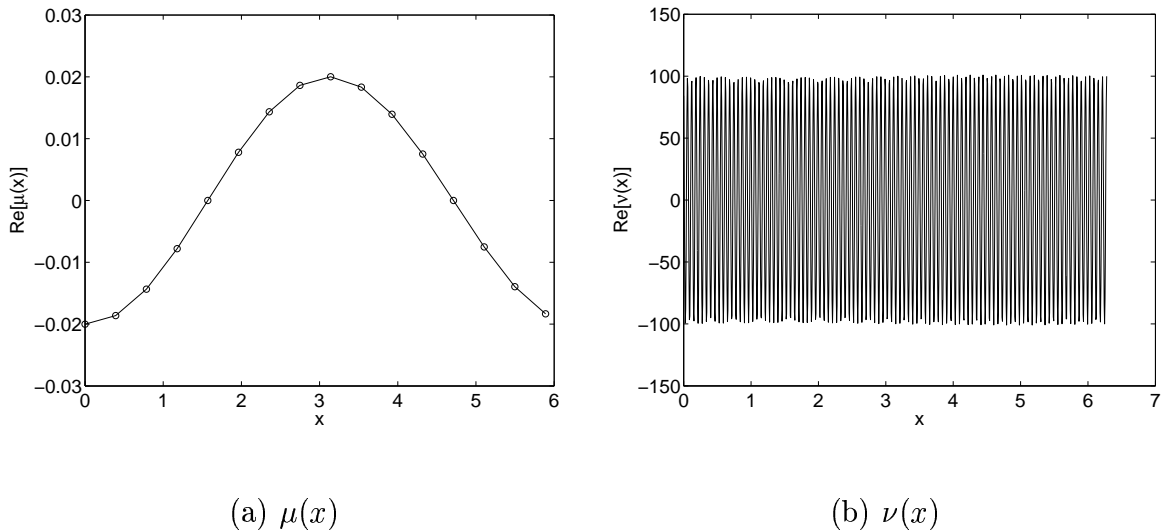


FIG. 2. Plots of the real parts of the slow surface velocity, $\mu(x)$, and fast surface velocity, $\nu(x)$. These plots are for the profile (24a) and $(\alpha = 100, \gamma = 100)$.

In Table IV we display results of FE, HFFE, OE, and HFOE simulations of plane-wave scattering from the sinusoidal profile, (24a), with various values of ε , $N_x = 16$, $N = 8$, and $(\alpha, \gamma) = (100, 100)$. The results in this table exemplify the broad range of applicability of our scheme within the setting of single scattering configurations. To determine the limits of our new approach, a simple geometrical acoustics calculation is needed to determine the first appearance of multiple reflection for the given incidence and grating shape. For instance, in the present case of the sinusoidal profile, (24a), and incident radiation $\alpha = \gamma$ we have determined that multiple reflections occur once $\varepsilon \approx 0.36$. By contrast, for the same profile but *normal* incidence, $\alpha = 0$, we found that secondary reflections occur at $\varepsilon \approx 0.82$.

In Table V we display results which illustrate the stabilizing effect which Padé summation can have on our algorithm. We again consider scattering from the cosine profile with incident radiation of frequency $(\alpha, \gamma) = (100, 100)$, but now focus on the largest value of ε presented thusfar ($\varepsilon = 0.1$) and compare, for values of the Taylor order $N = 0, \dots, 12$ (for a slightly larger $N_x = 32$ to avoid aliasing), the convergence of our high-frequency methods (HFFE and HFOE) with both Taylor and Padé summation. We see that through six orders all four calculations produce roughly the same precision, however, beyond eight orders the results from Taylor summation begin to deteriorate. This is particularly true for the HFOE algorithm, and highlights the advantageous properties of Padé summation even within the disk of convergence of these Taylor series.

We now present calculations for the Lipschitz profile, (25), (with $\varepsilon = 0.01$) which features Fourier series which decay very slowly (as r increases). Due to this extremely slow decay we found it necessary to choose $N_x = 256$ before our high-frequency algorithms gave uniformly good results. For this reason, the unmodified algorithms (FE and OE) were quite competitive up to $(\alpha, \gamma) = (10, 10)$ (see Tables VI and VII). However, once the frequency reached $(\alpha, \gamma) = (100, 100)$ our specially designed algorithms were clearly superior, see Table VIII. Again, the range of applicability of our algorithm is determined by the onset of multiple scattering events which, we have calculated, to set in at $\varepsilon \approx 0.42$ for $\alpha = \gamma$ and $\varepsilon \approx 0.91$ for normal incidence, $\alpha = 0$.

Finally, we make a comparison of our new methods to the Kirchhoff Approximation (KA) for these configurations. The results are summarized in Table IX and show that, while the KA does give improved results as the frequency is increased, it never approaches the accuracy of our new HFFE/HFOE algorithms.

B. Three Dimensional Test

We now present a set of illustrative numerical simulations to show that the HFFE and HFOE algorithms again deliver highly accurate solutions with very few degrees of freedom even in the three dimensional case of scattering by a crossed grating. For this set of experiments we consider the three dimensional smooth profile:

$$f_r^{(3)}(x_1, x_2) = \cos(x_1 - x_2) + \cos(2x_1 - 2x_2), \quad (26)$$

which is (2π) -periodic in both the x_1 and x_2 directions, and choose $\varepsilon = 0.01$ to avoid multiple reflections (see Figure 3). Again, we will use all four algorithms to compute the

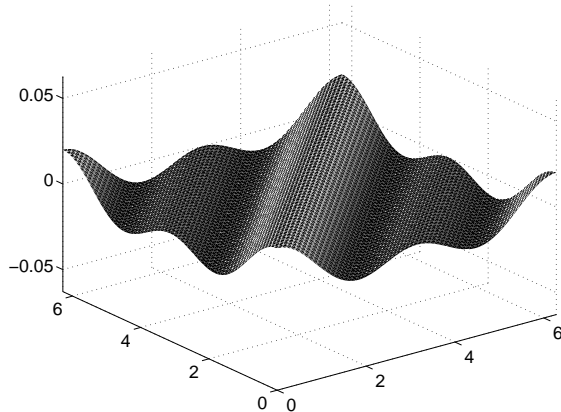


FIG. 3. Plot of the three-dimensional profile $f_r^{(3)}(x_1, x_2)$, (26).

normal derivative of the field at the surface of the scatterer and compare this with a highly resolved TFE simulation, again accurate to around 10^{-10} ($N_{x_1} = 128$, $N_{x_2} = 128$, $N_y = 64$, $N = 28$). We display results of these simulations with $N_{x_1} = 32$, $N_{x_2} = 32$, and Taylor orders $N = 0, 2, 4, 6$, and 8 in Tables X, XI, and XII for $(\alpha, \beta, \gamma) = (1, 1, 1)$, $(10, 10, 10)$, and $(100, 100, 100)$, respectively.

For a relatively small frequency, $(\alpha, \beta, \gamma) = (1, 1, 1)$, all four algorithms work very well, c.f. Table X. However, at the more moderate frequency $(\alpha, \beta, \gamma) = (10, 10, 10)$ the standard FE/OE methods become disadvantaged and can only resolve the normal derivative of the field to 10^{-5} , see Table XI. Finally, once we reach the relatively high frequency $(\alpha, \beta, \gamma) = (100, 100, 100)$ the FE/OE approaches produce inaccurate results while the HFFE and HFOE methods produce solutions which are accurate to 10^{-10} .

To close, we note, for sake of comparison, that the KA delivers solutions with errors 0.0652607, 0.0106076, 0.000975237 for $(\alpha, \beta, \gamma) = (1, 1, 1)$, $(10, 10, 10)$, and $(100, 100, 100)$, respectively. Again, these errors are decreasing as the frequency is increased, but the KA solution cannot compete with the ones that HFFE/HFOE produce.

V. CONCLUSIONS

In this paper we have shown how asymptotic phase information can be incorporated into high-order boundary perturbation methods to produce numerical algorithms for acoustic scattering which are error-controllable with frequency-independent computational cost. A detailed specification has been given for two particularly popular boundary perturbation schemes, the ‘‘Field Expansions’’ method, based on perturbative expansions of the pressure, and the ‘‘Operator Expansion’’ method which works with expansions of the relevant Dirichlet–Neumann operator. Of particular note, these new methods *never* produce significantly worse results than the original FE/OE recursions, regardless of the frequency. Therefore it appears that these high-frequency schemes are to be recommended for *all* configurations where FE and OE are applicable. Also, provided that we have properly resolved the profile, there is *always* a smallest frequency for which these new methods are significantly more accurate than the standard FE/OE algorithms. Furthermore, for frequencies larger than this critical value the FE/OE recursions become unreliable while our new procedures produce consistently accurate results. In this first contribution we have restricted our descriptions and numerical results to geometries which do not generate multiple reflections.

However, we have discussed how these single-reflection methods can be rendered applicable to multiple scattering configurations, though we leave the specification and implementation to future work.

Acknowledgments

DPN gratefully acknowledges support from the NSF through grant No. DMS-0537511. FR gratefully acknowledges support from AFOSR through contract No. FA9550-05-1-0019 and from NSF through grant No. DMS-0311763.

Disclaimer. Effort sponsored by the Air Force Office of Scientific Research, Air Force Materials Command, USAF, under grant number FA9550-05-1-0019. The US Government is authorized to reproduce and distribute reprints for governmental purposes notwithstanding any copyright notation thereon. The views and conclusions contained herein are those of the author and should not be interpreted as necessarily representing the official policies or endorsements, either expressed or implied, of the Air Force Office of Scientific Research or the US Government.

References

- ¹ L. Tsang, J. A. Kong, and R. T. Shin, *Theory of Microwave Remote Sensing* (Wiley, New York) (1985).
- ² P. J. Shull, *Nondestructive Evaluation: Theory, Techniques, and Applications* (Marcel Dekker) (2002).
- ³ F. Natterer and F. Wübbeling, *Mathematical methods in image reconstruction*, SIAM Monographs on Mathematical Modeling and Computation (Society for Industrial and Applied Mathematics (SIAM), Philadelphia, PA) (2001).
- ⁴ J. Ogilvy, *Theory of Wave Scattering from Random Rough Surfaces* (Institute of Physics Publishing) (1991).

- ⁵ P. Lynch, “Curvature corrections to rough-surface scattering at high frequencies”, *J. Acoust. Soc. Am.* **47**, 804–815 (1970).
- ⁶ E. Liszka and J. McCoy, “Scattering at a rough boundary—extensions of the Kirchhoff approximation”, *J. Acoust. Soc. Am.* **71**, 1093–1100 (1982).
- ⁷ H. Chaloupka and H. Meckelburg, “Improved high-frequency current approximation for curved conducting surfaces”, *Arch. Elektron. bertragungstech.* **39**, 245–250 (1985).
- ⁸ E. Rodriguez, “Beyond the Kirchhoff approximation”, *Radio Sci.* **24**, 681–693 (1989).
- ⁹ O. P. Bruno and F. Reitich, “Numerical solution of diffraction problems: A method of variation of boundaries”, *J. Opt. Soc. Am. A* **10**, 1168–1175 (1993).
- ¹⁰ O. P. Bruno and F. Reitich, “Numerical solution of diffraction problems: A method of variation of boundaries. II. Finitely conducting gratings, Padé approximants, and singularities”, *J. Opt. Soc. Am. A* **10**, 2307–2316 (1993).
- ¹¹ O. P. Bruno and F. Reitich, “Numerical solution of diffraction problems: A method of variation of boundaries. III. Doubly periodic gratings”, *J. Opt. Soc. Am. A* **10**, 2551–2562 (1993).
- ¹² O. P. Bruno and F. Reitich, “Calculation of electromagnetic scattering via boundary variations and analytic continuation”, *Appl. Comput. Electromagn. Soc. J.* **11**, 17–31 (1996).
- ¹³ O. P. Bruno and F. Reitich, “Boundary–variation solutions for bounded–obstacle scattering problems in three dimensions”, *J. Acoust. Soc. Am.* **104**, 2579–2583 (1998).
- ¹⁴ O. P. Bruno and F. Reitich, “High-order boundary perturbation methods”, in *Mathematical Modeling in Optical Science*, volume 22, 71–109 (SIAM, Philadelphia, PA) (2001), frontiers in Applied Mathematics Series.
- ¹⁵ D. P. Nicholls and F. Reitich, “Shape deformations in rough surface scattering: Cancellations, conditioning, and convergence”, *J. Opt. Soc. Am. A* **21**, 590–605 (2004).
- ¹⁶ D. P. Nicholls and F. Reitich, “Shape deformations in rough surface scattering: Improved algorithms”, *J. Opt. Soc. Am. A* **21**, 606–621 (2004).
- ¹⁷ J. Cullen, “Surface currents induced on short-wavelength radiation”, *Physical Review*

- 109**, 1863–1867 (1958).
- ¹⁸ V. Fock, *Electromagnetic Diffraction and Propagation Problems*, volume 1 of *International Series of Monographs on Electromagnetic Waves* (Pergamon Press, Oxford) (1965).
- ¹⁹ A. G. Voronovich, *Wave scattering from rough surfaces*, second edition (Springer-Verlag, Berlin) (1999).
- ²⁰ M. Charnotskii and V. Tatarskii, “Tilt-invariant theory of rough surface scattering”, *Waves Random Media* **5**, 361–380 (1995).
- ²¹ O. Bruno, A. Sei, and M. Caponi, “High-order high-frequency solutions of rough surface scattering problems”, *Radio Science* **37**, 1–13 (2002).
- ²² F. Reitich and C. Turc, “High-order solutions of three-dimensional rough-surface scattering problems at high frequencies. I. The scalar case”, *Waves Random Complex Media* **15**, 1–16 (2005).
- ²³ F. Reitich and C. Turc, “High-order solutions of three-dimensional rough-surface scattering problems at high-frequencies. II. The vector electromagnetic case”, *Waves Random Complex Media* **15**, 323–337 (2005).
- ²⁴ O. P. Bruno, C. A. Geuzaine, J. A. Munro, and F. Reitich, “Prescribed error tolerances within fixed computational times for scattering problems of arbitrarily high frequency: The convex case”, *Phil. Trans. R. Soc. Lond. A* **362**, 629–645 (2004).
- ²⁵ O. Bruno, C. Geuzaine, and F. Reitich, “A new high-order high-frequency integral equation method for the solution of scattering problems. ii: Multiple-scattering configurations”, in *Proceedings of the 20th Annual Review of Progress in Applied Computational Electromagnetics, ACES 2004* (2004).
- ²⁶ C. Linton, “The Green’s function for the two-dimensional Helmholtz equation in periodic domains”, *J. Eng. Math.* **33**, 377–402 (1998).
- ²⁷ L. Rayleigh, “On the dynamical theory of gratings”, *Proc. Roy. Soc. London* **A79**, 399–416 (1907).
- ²⁸ S. O. Rice, “Reflection of electromagnetic waves from slightly rough surfaces”, *Comm. Pure Appl. Math.* **4**, 351–378 (1951).

- ²⁹ D. M. Milder, “An improved formalism for rough-surface scattering of acoustic and electromagnetic waves”, in *Proceedings of SPIE - The International Society for Optical Engineering (San Diego, 1991)*, volume 1558, 213–221 (Int. Soc. for Optical Engineering, Bellingham, WA) (1991).
- ³⁰ D. M. Milder, “An improved formalism for wave scattering from rough surfaces”, *J. Acoust. Soc. Am.* **89**, 529–541 (1991).
- ³¹ D. M. Milder and H. T. Sharp, “Efficient computation of rough surface scattering”, in *Mathematical and numerical aspects of wave propagation phenomena (Strasbourg, 1991)*, 314–322 (SIAM, Philadelphia, PA) (1991).
- ³² D. M. Milder and H. T. Sharp, “An improved formalism for rough surface scattering. ii: Numerical trials in three dimensions”, *J. Acoust. Soc. Am.* **91**, 2620–2626 (1992).
- ³³ D. M. Milder, “Role of the admittance operator in rough-surface scattering”, *J. Acoust. Soc. Am.* **100**, 759–768 (1996).
- ³⁴ S. N. Chandler-Wilde and B. Zhang, “Electromagnetic scattering by an inhomogeneous conducting or dielectric layer on a perfectly conducting plate”, *R. Soc. Lond. Proc. Ser. A Math. Phys. Eng. Sci.* **454**, 519–542 (1998).
- ³⁵ J. B. Keller and D. Givoli, “Exact nonreflecting boundary conditions”, *J. Comput. Phys.* **82**, 172–192 (1989).
- ³⁶ F. Ihlenburg, *Finite element analysis of acoustic scattering* (Springer-Verlag, New York) (1998).
- ³⁷ O. P. Bruno and F. Reitich, “Solution of a boundary value problem for the Helmholtz equation via variation of the boundary into the complex domain”, *Proc. Roy. Soc. Edinburgh Sect. A* **122**, 317–340 (1992).
- ³⁸ D. P. Nicholls and F. Reitich, “Analytic continuation of Dirichlet-Neumann operators”, *Numer. Math.* **94**, 107–146 (2003).
- ³⁹ G. A. Baker, Jr. and P. Graves-Morris, *Padé approximants*, second edition (Cambridge University Press, Cambridge) (1996).
- ⁴⁰ R. B. Melrose and M. E. Taylor, “Near peak scattering and the corrected Kirchhoff

approximation for a convex obstacle”, *Adv. in Math.* **55**, 242–315 (1985).

- ⁴¹ D. P. Nicholls and F. Reitich, “A new approach to analyticity of Dirichlet-Neumann operators”, *Proc. Roy. Soc. Edinburgh Sect. A* **131**, 1411–1433 (2001).

TABLE I. Relative error in FE, OE, HFFE, and HFOE algorithms (all with $N_x = 16$) versus perturbation order N for the cosine profile, (24a), as compared to a highly resolved TFE simulation ($N_x = 1024$, $N_y = 64$, $N = 28$); frequency is ($\alpha = 1, \gamma = 1$).

N	FE	HFFE	OE	HFOE
0	9.91×10^{-3}	1.57×10^{-2}	9.91×10^{-3}	1.57×10^{-2}
2	1.37×10^{-6}	8.8×10^{-7}	1.37×10^{-6}	8.8×10^{-7}
4	3.53×10^{-10}	3.66×10^{-10}	3.53×10^{-10}	3.66×10^{-10}
6	3.53×10^{-10}	3.53×10^{-10}	3.53×10^{-10}	3.53×10^{-10}
8	3.53×10^{-10}	3.53×10^{-10}	3.53×10^{-10}	3.53×10^{-10}

TABLE II. Relative error in FE, OE, HFFE, and HFOE algorithms (all with $N_x = 16$) versus perturbation order N for the cosine profile, (24a), as compared to a highly resolved TFE simulation ($N_x = 1024$, $N_y = 64$, $N = 28$); frequency is ($\alpha = 10$, $\gamma = 10$).

N	FE	HFFE	OE	HFOE
0	2×10^0	1.01×10^{-2}	2×10^0	1.01×10^{-2}
2	2×10^0	6.31×10^{-7}	2×10^0	6.31×10^{-7}
4	2×10^0	1.99×10^{-8}	2×10^0	1.99×10^{-8}
6	2×10^0	1.07×10^{-10}	2×10^0	1.07×10^{-10}
8	2×10^0	3.62×10^{-11}	2×10^0	3.62×10^{-11}

TABLE III. Relative error in FE, OE, HFFE, and HFOE algorithms (all with $N_x = 16$) versus perturbation order N for the cosine profile, (24a), as compared to a highly resolved TFE simulation ($N_x = 1024$, $N_y = 64$, $N = 28$); frequency is ($\alpha = 100$, $\gamma = 100$).

N	FE	HFFE	OE	HFOE
0	2×10^0	9.9×10^{-3}	2×10^0	9.9×10^{-3}
2	2×10^0	2.33×10^{-8}	2×10^0	2.33×10^{-8}
4	2×10^0	5.97×10^{-12}	2×10^0	5.97×10^{-12}
6	2×10^0	5.97×10^{-12}	2×10^0	5.97×10^{-12}
8	2×10^0	5.97×10^{-12}	2×10^0	5.97×10^{-12}

TABLE IV. Relative error in FE, OE, HFFE, and HFOE algorithms (all with $N_x = 16$, $N = 8$) versus perturbation size ε , for the cosine profile, (24a), as compared to a TFE simulation ($N_x = 1024$, $N_y = 64$, $N = 28$); frequency is ($\alpha = 100, \gamma = 100$).

ε	FE	HFFE	OE	HFOE
0.02	2.01×10^0	2.9×10^{-12}	2.01×10^0	3.07×10^{-12}
0.03	2.06×10^0	4.01×10^{-12}	2.06×10^0	6.05×10^{-12}
0.04	2.22×10^0	5.63×10^{-12}	2.17×10^0	4.01×10^{-11}
0.05	2.33×10^0	9.8×10^{-12}	2.25×10^0	1.9×10^{-10}
0.06	2.34×10^0	2.09×10^{-11}	2.25×10^0	7.36×10^{-10}
0.07	2.21×10^0	5.72×10^{-11}	2.16×10^0	2.33×10^{-9}
0.08	2.53×10^0	7.73×10^{-10}	2.16×10^0	5.21×10^{-9}
0.09	2.23×10^0	2.21×10^{-9}	2.13×10^0	8.2×10^{-9}
0.1	2.13×10^0	1.83×10^{-9}	2.11×10^0	1.14×10^{-8}

TABLE V. Relative error in HFFE and HFOE algorithms summed via Taylor and Padé algorithms (all with $N_x = 32$) versus perturbation order N for the cosine profile, (24a), as compared to a highly resolved TFE simulation ($N_x = 1024$, $N_y = 64$, $N = 28$); frequency is ($\alpha = 100$, $\gamma = 100$).

N	HFFE (Taylor)	HFFE (Padé)	HFOE (Taylor)	HFOE (Padé)
0	9.09×10^{-2}	9.09×10^{-2}	9.09×10^{-2}	9.09×10^{-2}
2	2.38×10^{-5}	2.38×10^{-5}	2.38×10^{-5}	2.38×10^{-5}
4	3.12×10^{-7}	2.85×10^{-8}	3.13×10^{-7}	2.85×10^{-8}
6	4.46×10^{-9}	2.1×10^{-9}	2.17×10^{-8}	4.86×10^{-8}
8	1.25×10^{-8}	4.22×10^{-9}	1.09×10^{-5}	4.88×10^{-8}
10	5.88×10^{-7}	2.16×10^{-9}	6.47×10^{-3}	3.26×10^{-8}
12	4.17×10^{-5}	1.54×10^{-8}	2.33×10^0	2.89×10^{-8}

TABLE VI. Relative error in FE, OE, HFFE, and HFOE algorithms (all with $N_x = 256$) versus perturbation order N for the Lipschitz profile, (25), as compared to a highly resolved TFE simulation ($N_x = 1024$, $N_y = 64$, $N = 28$); frequency is ($\alpha = 1$, $\gamma = 1$).

N	FE	HFFE	OE	HFOE
0	2.02×10^{-2}	3.6×10^{-2}	2.02×10^{-2}	3.6×10^{-2}
2	9.59×10^{-6}	1.32×10^{-6}	9.59×10^{-6}	1.32×10^{-6}
4	3.5×10^{-10}	3.55×10^{-10}	3.55×10^{-10}	3.55×10^{-10}
6	3.46×10^{-10}	3.46×10^{-10}	3.64×10^{-10}	3.46×10^{-10}
8	3.46×10^{-10}	3.46×10^{-10}	3.75×10^{-10}	3.46×10^{-10}
10	3.46×10^{-10}	3.46×10^{-10}	3.72×10^{-10}	3.46×10^{-10}
12	3.46×10^{-10}	3.46×10^{-10}	3.72×10^{-10}	3.46×10^{-10}

TABLE VII. Relative error in FE, OE, HFFE, and HFOE algorithms (all with $N_x = 256$) versus perturbation order N for the Lipschitz profile, (25), as compared to a highly resolved TFE simulation ($N_x = 1024$, $N_y = 64$, $N = 28$); frequency is ($\alpha = 10$, $\gamma = 10$).

N	FE	HFFE	OE	HFOE
0	1.06×10^{-2}	1.79×10^{-2}	1.06×10^{-2}	1.79×10^{-2}
2	1.31×10^{-4}	8.97×10^{-6}	1.31×10^{-4}	8.97×10^{-6}
4	1.82×10^{-10}	2.96×10^{-8}	1.85×10^{-10}	2.96×10^{-8}
6	4.04×10^{-11}	4.54×10^{-11}	6.06×10^{-11}	4.54×10^{-11}
8	4.04×10^{-11}	4.17×10^{-11}	7.3×10^{-11}	4.17×10^{-11}
10	4.05×10^{-11}	4.1×10^{-11}	6.97×10^{-11}	4.1×10^{-11}
12	4.05×10^{-11}	4.1×10^{-11}	6.99×10^{-11}	4.1×10^{-11}

TABLE VIII. Relative error in FE, OE, HFFE, and HFOE algorithms (all with $N_x = 256$) versus perturbation order N for the Lipschitz profile, (25), as compared to a highly resolved TFE simulation ($N_x = 1024$, $N_y = 64$, $N = 28$); frequency is ($\alpha = 100$, $\gamma = 100$).

N	FE	HFFE	OE	HFOE
0	2.02×10^{-3}	8.08×10^{-3}	2.02×10^{-3}	8.08×10^{-3}
2	1.2×10^{-3}	9.01×10^{-6}	1.2×10^{-3}	9.01×10^{-6}
4	1.2×10^{-3}	1.73×10^{-5}	1.2×10^{-3}	1.73×10^{-5}
6	1.2×10^{-3}	2.78×10^{-7}	1.2×10^{-3}	2.78×10^{-7}
8	1.2×10^{-3}	3.57×10^{-9}	1.2×10^{-3}	3.57×10^{-9}
10	1.2×10^{-3}	3.21×10^{-10}	1.2×10^{-3}	3.22×10^{-10}
12	1.2×10^{-3}	2.71×10^{-10}	1.2×10^{-3}	2.72×10^{-10}

TABLE IX. Relative error in Kirchhoff Approximation for cosine, (24a) and Lipschitz profiles, (25), as compared to a highly resolved TFE simulation ($N_x = 1024$, $N_y = 64$, $N = 28$).

Profile	$(\alpha, \gamma) = (1, 1)$	$(\alpha, \gamma) = (10, 10)$	$(\alpha, \gamma) = (100, 100)$
cosine	0.0197672	0.00201072	0.000198089
Lipschitz	0.0403573	0.0210931	0.00368225

TABLE X. Relative error in FE, OE, HFFE, and HFOE algorithms (all with $N_{x_1} = 32$ and $N_{x_2} = 32$) versus perturbation order N for the three dimensional smooth profile, (26), as compared to a highly resolved TFE simulation ($N_{x_1} = 128$, $N_{x_2} = 128$, $N_y = 64$, $N = 28$); frequency is ($\alpha = 1, \beta = 1, \gamma = 1$).

N	FE	HFFE	OE	HFOE
0	3.25×10^{-2}	5.25×10^{-2}	3.25×10^{-2}	5.25×10^{-2}
2	3.78×10^{-5}	3.77×10^{-5}	3.78×10^{-5}	3.77×10^{-5}
4	2.79×10^{-9}	2.1×10^{-8}	2.79×10^{-9}	2.1×10^{-8}
6	1.62×10^{-10}	1.62×10^{-10}	1.62×10^{-10}	1.62×10^{-10}
8	1.61×10^{-10}	1.61×10^{-10}	1.61×10^{-10}	1.61×10^{-10}

TABLE XI. Relative error in FE, OE, HFFE, and HFOE algorithms (all with $N_{x_1} = 32$ and $N_{x_2} = 32$) versus perturbation order N for the three dimensional smooth profile, (26), as compared to a highly resolved TFE simulation ($N_{x_1} = 128, N_{x_2} = 128, N_y = 64, N = 28$); frequency is ($\alpha = 10, \beta = 10, \gamma = 10$).

N	FE	HFFE	OE	HFOE
0	5.34×10^{-3}	2.99×10^{-2}	5.34×10^{-3}	2.99×10^{-2}
2	7.39×10^{-4}	3.89×10^{-4}	7.39×10^{-4}	3.89×10^{-4}
4	5.3×10^{-5}	7.03×10^{-6}	5.3×10^{-5}	7.03×10^{-6}
6	5.3×10^{-5}	1.79×10^{-8}	5.3×10^{-5}	1.79×10^{-8}
8	5.3×10^{-5}	5.56×10^{-11}	5.3×10^{-5}	5.56×10^{-11}

TABLE XII. Relative error in FE, OE, HFFE, and HFOE algorithms (all with $N_{x_1} = 32$ and $N_{x_2} = 32$) versus perturbation order N for the three dimensional smooth profile, (26), as compared to a highly resolved TFE simulation ($N_{x_1} = 128, N_{x_2} = 128, N_y = 64, N = 28$); frequency is ($\alpha = 100, \beta = 100, \gamma = 100$).

N	FE	HFFE	OE	HFOE
0	1.21×10^0	2.66×10^{-2}	1.21×10^0	2.66×10^{-2}
2	1.21×10^0	1.29×10^{-6}	1.21×10^0	1.29×10^{-6}
4	1.21×10^0	4.33×10^{-10}	1.21×10^0	4.33×10^{-10}
6	1.21×10^0	1.43×10^{-10}	1.21×10^0	1.48×10^{-10}
8	1.21×10^0	1.43×10^{-10}	1.21×10^0	1.51×10^{-10}

List of Figures

FIG. 1	Plots of the two-dimensional profiles $f_s(x) = \cos(x)$, (24a), and $f_{L,40}$, (25).	18
FIG. 2	Plots of the real parts of the slow surface velocity, $\mu(x)$, and fast surface velocity, $\nu(x)$. These plots are for the profile (24a) and $(\alpha = 100, \gamma = 100)$.	19
FIG. 3	Plot of the three-dimensional profile $f_r^{(3)}(x_1, x_2)$, (26).	21